A Study of Plasmonic Properties of a Rhodium I-shaped Nanomaterial

Yaru SHI [1], Yue ZHANG [1], Wei WANG [1, 2], Tao XIONG [1, 2], Dandan DONG [1, 2], Cheng SUN [1, 2] *

[1] *College of Physical Science and Technology, Dalian University, 116622, China*
[2] *Liaoning Engineering Laboratory of Optoelectronic Information Technology, Dalian, 116622, China*

In this work, the optical properties of a rhodium I-shaped nanomaterial are studied. In the UV-visible regime, the scattering efficiency and the electric field are calculated via the finite-difference time-domain method, with the parameters varying including the height, the length ratio, and the polarization of the incident light. The results show that multiple resonance peaks are observed in the scattering spectrum in the ultraviolet region, corresponding to different electromagnetic modes. It is also revealed that the peak strength of the nanostructure can be effectively tuned by adjusting the structural parameters. The proposed rhodium nanomaterial may provide a theoretical basis for the design of optical devices in the ultraviolet regime. The obtained results provide useful guidance for the implementation of nanoantenna and fluorescence enhancement, etc.

Keywords: rhodium I-shape nanostructure, ultraviolet, finite difference time domain, scattering spectrum.

1. INTRODUCTION

Under the excitation of incident light, the free electrons on the surface of noble metals oscillate collectively, and surface plasmons are induced [1, 2]. The corresponding optical properties and electromagnetic fields can be utilized in applications of sensors, optical waveguides, subwavelength optics, and nonlinear science, etc [3 – 6].

So far, nanomaterials with specific symmetries have been shown to possess great plasmonic properties [7]. For example, the influence of surrounding dielectric materials on the capacitive coupling strength of the H-shaped plasmonic subsurface has been reported [8]. The plasmonic properties of the V-shaped gold nanostructures were studied, and the resonance intensity was controlled by changing the angle of the "V" arm [9]. In addition, the influence of the geometric parameters of the E-shaped plasmonic nanocavities on the optical properties was also discussed [10]. Recently, a design of a Y-shaped plasmonic tripod nanostructure was proposed and properties were addressed [11].

Today, plasmonic metals that are widely studied include silver, gold, and copper, etc., whose spectral ranges fall mainly in the visible and near-infrared regions [12]. However, with increasing demand for devices in the ultraviolet (UV) regime and the continuous exploration of the UV scientific research, the study of plasmonic noble metals in the UV range becomes more significant. Therefore, it is important to find metals with excellent properties in the UV spectrum. Among many promising metals, rhodium has been shown to have a good plasmonic response in the UV regime [13, 14]. For instance, it has been shown that the surrounding field strength and charge density of rhodium nanocubes can be effectively regulated, by changing their edge shape [15]. The optical properties and application in the catalysis of rhodium in the UV region

were also reported [16, 17]. An antenna consisting of a rhodium nanoring dimer was designed for biochemical sensing, and the plasmonic resonance was effectively mixed in the deep UV region [18]. Furthermore, the plasmonic properties and application of surface-enhanced Raman scattering (SERS) of rhodium were also explored [19]. Besides, a nanoantenna consisting of a pair of aluminum truncated hollow triangles to support the Fano-like resonant mode in the near-UV band, which paves new promising strategies to design efficient UV-based plasmonic devices [20].

In this work, an I-shaped rhodium nanomaterial is investigated. In contrast to previous work, the present work has a response range in the UV region, the resonance wavelength that is studied is this work is smaller; besides, the proposed I-shape structure can be tuned in multiple dimensions with a relatively more comprehensive tuning of its structural parameters, compared to the V-shaped structure that changes the angle of the "V" arm singularly. In contrast to other works on rhodium-based structures, a highly symmetric I-shaped nanostructure is used to probe plasmonic resonance effects in the UV- visible range in this work. The light scattering properties of this I-shaped nanomaterial are significantly dependent on the structural parameters. The symmetrical splicing structure facilitates the generation of multi-band resonance peaks and the enhancement of local electromagnetic fields. We suggest that the I-shaped structure may play a role in spectrally selective filters, metal-enhanced fluorescence, etc. The scattering efficiency and electric field distribution in the UV-visible region are probed and quantitatively analyzed. The plasmonic resonances related to different electromagnetic modes are also discussed. The structure is demonstrated to be well adjustable, and the plasmonic wavelength in the UV region can be tuned by changing the length of the rhodium nano bar.

---

* Corresponding author. Tel.: +86-411-87402712;
fax: +86-411-87402712. E-mail: *suncheng@dlu.edu.cn* (C. Sun)

2. STRUCTURE AND METHOD

The structure of the I-shape rhodium nanomaterial proposed in this paper is shown in Fig. 1. Referring to Fig. 1, an I-shaped structure consisting of two bars and a post was placed in the *x-y* plane. The widths of the top and bottom bars are indicated in w_t and w_b, respectively, and the height of the post is labeled *h*. The cross sections of the bars and the post were all squared, and the area was fixed to be of $d \times d = 10 \times 10$ nm^2. The incident light was a plane-wave light, which was incident along the *z*-axis. The polarization angle is indicated in φ_p, which is the angle between the electric vector of the light and the *x*-axis.

In this work, the finite-difference time-domain method (FDTD) was used for all simulations [21], and the perfect matching layer (PML) boundary condition was adopted in all directions. The studied wavelength range of the incident light was $100 - 800$ nm. The optical constants of rhodium were from Palik's experimental data [22]. Note that the results are obtained by numerical simulation only. And yet, as addressed in [23], the experimental results of a symmetric structure are consistent with simulations, and it is reasonable to assume the structure proposed in this work can also be produced and verified experimentally. However, the results given in this work should still be used with caution.
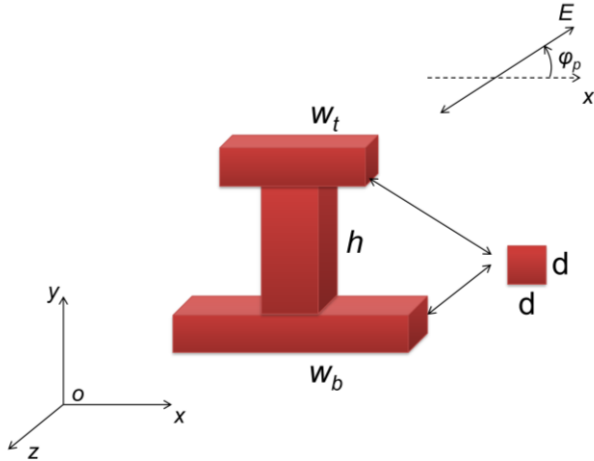
Fig. 1. The structure of the I-shaped nanomaterial consisting of rhodium. The width of the top bar is w_t, the width of the bottom bar is w_b, and the height of the post is *h*. The cross sections of the bars and the post are all squared, with a fixed area of $d \times d$. The polarization of incident light is expressed by φ_p, which is the angle between the electric vector and the *x*-axis

3. RESULTS AND DISCUSSION

### 3.1. Effects of the post's height

According to the structure shown in Fig. 1, the scattering efficiency was calculated by the following equation:

$$\text{Scattering efficiency} = C_{scat}/S, \tag{1}$$

where C_{scat} is the scattering cross-section of the nanostructure; S is the projected cross-sectional area of the incident light in the x-y plane. First, the top and bottom bars of the I-shaped rhodium nanostructure were kept constant to be $w_t = 30$ nm and $w_b = 50$ nm, while the height of the post

was increased from 50 to 110 nm. The scattering efficiency was simulated and the results are given in Fig. 2 a. As can be seen in Fig. 2 a, two distinguishable peaks occur in the UV-visible region from 100 to 400 nm, indicating two obvious plasmonic resonances. For simplicity, the peak at the shorter wavelength is labeled as A, and the peak at the longer wavelength is labeled as B. Based on Fig. 1 the resonance wavelengths of peaks A and B were respectively determined, and the results are plotted in Fig. 2 b. According to Fig. 2 b, with the increase of height, peak B shows a redshift trend from 310 to 350 nm, while peak A maintains a constant of about 160 nm. This infers that these two peaks may correspond to two different resonance modes.

To distinguish the electromagnetic modes of peaks A and B, the electric field distributions in the *x-y* plane were calculated, and an exemplary result is shown in Fig. 3 when the height was $h = 80$ nm. According to Fig. 3 a, the electric field of peak A is mainly confined at both sides of the post of the I-shape rhodium. However, it can be seen from Fig. 3 b that the field occurs in the spatial region that is close to the bars. By comparing Fig. 3 a and b, it is obvious that peak A and peak B have two different electric field distributions, corresponding to two plasmonic modes.
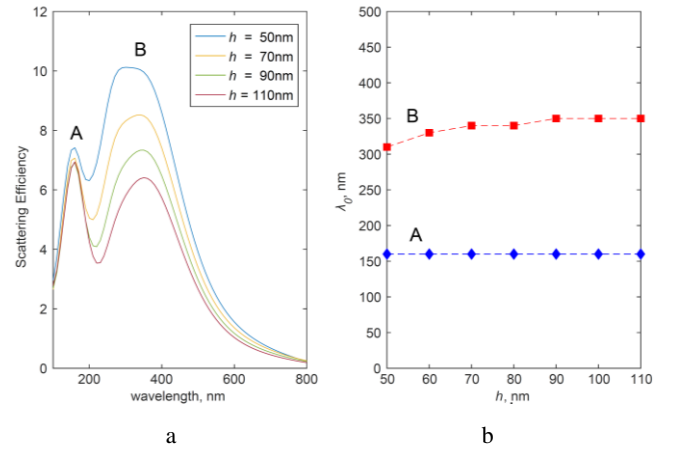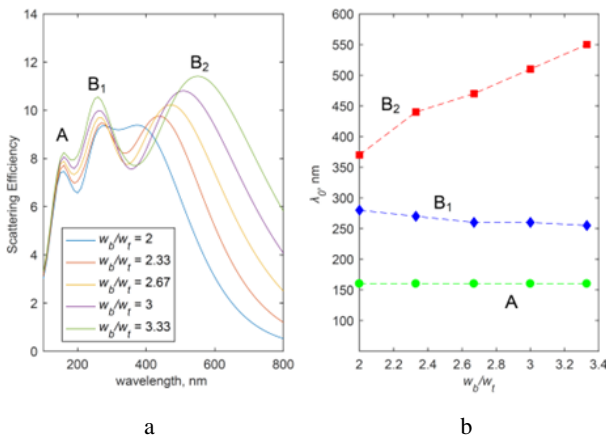

Fig. 2. a – scattering efficiency as a function of wavelength at different heights of the post; b – resonance wavelength (λ_0) as a function of the height. In the simulations $w_t = 30$ nm and $w_b = 50$ nm. The incident light was *x*-polarized
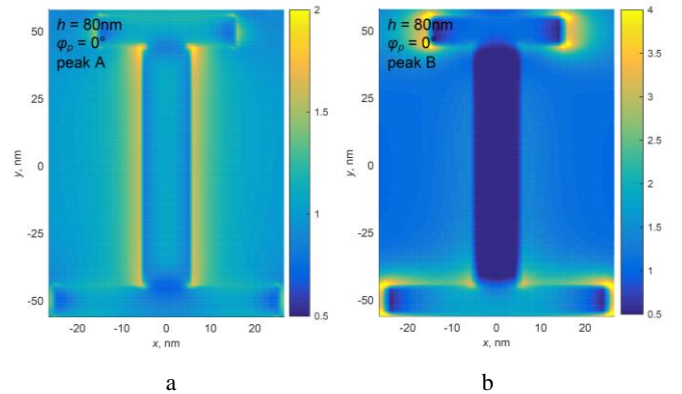
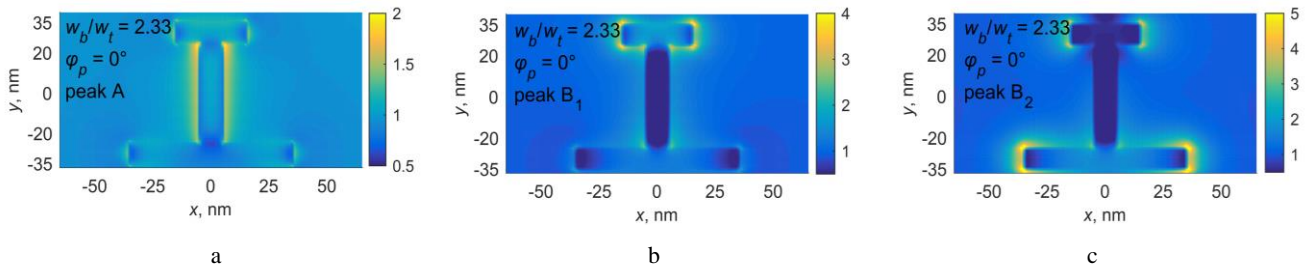**Fig. 3.** Electric field distribution in the *x-y* plane with $h = 80$ nm: a – peak A; b – peak B

3.2. Effects of the width ratio of bottom bar to top bar

Below, the width ratio of w_b/w_t was varied from 2 to 3.33, by changing the width of the bottom bar from 60 to 100 nm, while keeping the width of the top bar to be 30 nm. The scattering efficiency was computed and the resulting curves are shown in Fig. 4 a. Regarding Fig. 4 a, three groups of peaks appear near 160 nm, 280 nm, and between 370 and 550 nm, respectively. For simplicity, they are denoted in A, B_1 and B_2, respectively. Based on the peaks, the values of the resonance wavelengths were determined, and the results are plotted in Fig. 4 b. It is observed from Fig. 4 b that with increasing width ratio, peak A remains unchanged at 160 nm. Peak B_1 shows a slight blueshift from 280 to 255 nm, whereas peak B_2 presents a pronounced redshift from 370 to 550 nm.

a   b

Fig. 4. a – scattering efficiency as a function of wavelength at different width ratios of bottom bar to top bar; b – resonance wavelength (λ_0) as a function of the width ratio. In the simulations $w_t = 30$ nm and $h = 50$ nm. w_b was varied from 60 to 100 nm so that w_b/w_t was changed from 2 to 3.33. The incident light was x-polarized

To understand the underlying physics of the trends shown in Fig. 4, the electric field distributions were further calculated, and the results of $w_b/w_t = 2.33$ are shown in Fig. 5 as an example. In Fig. 5, the values of 160, 270, and 440 nm were used, corresponding to the resonance wavelengths of peaks A, B_1 and B_2, respectively. As indicated in Fig. 5 a, the electric field of peak A surrounds mainly the sides of the post; this is similar to the field distribution observed in Fig. 3 a. In Fig. 5 b the field of peak B_1 appears only on the surface of the top bar, while that of peak B_2 in Fig. 5 c is dominated by the bottom bar. It is clear

from Fig. 5 that the three peaks have different electromagnetic field distributions, corresponding to three plasmonic modes.

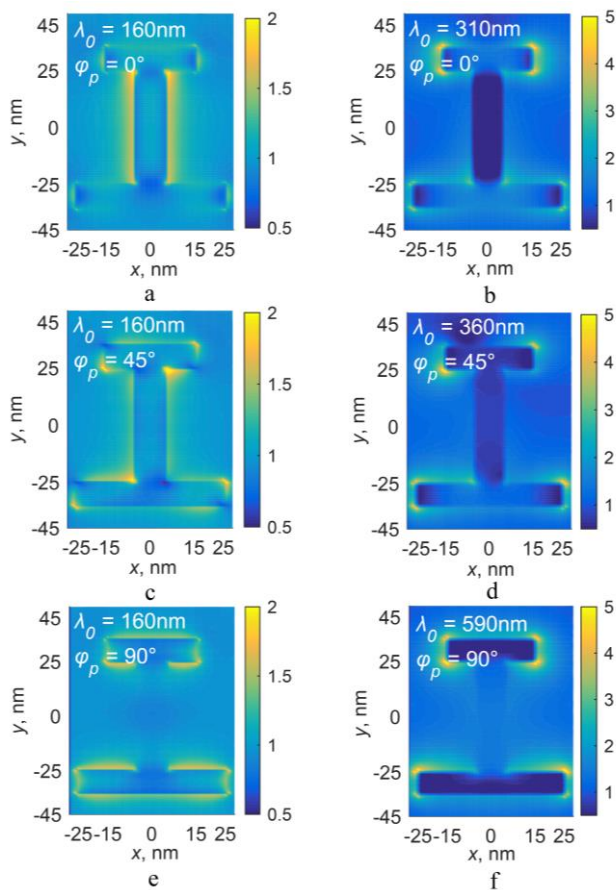## 3.3. Effects of the light's polarization

As is known to the community, in addition to the size of the plasmonic nanostructures, the polarization of incident light is also an important parameter that may affect the plasmonic properties of the system [24]. In this work, the polarization effects of the I-shaped rhodium were also probed, and the scattering efficiency was computed when the size was fixed to be $h = 50$ nm, $w_t = 30$ nm and $w_b = 50$ nm; the resultant curves are illustrated in Fig. 6.
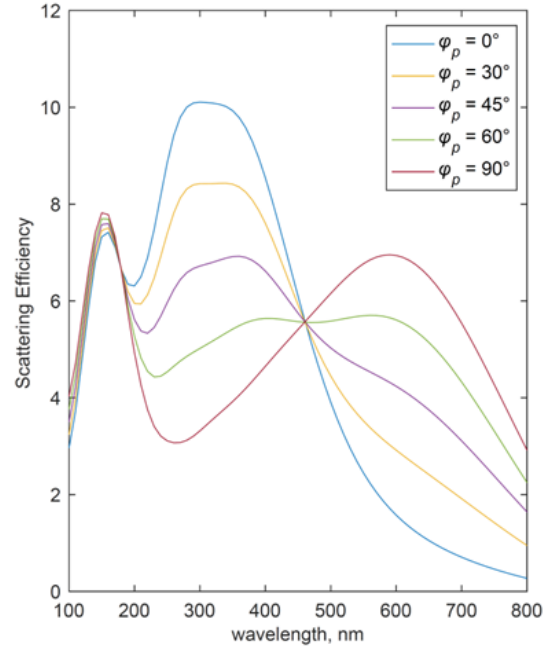
Fig. 6. Scattering efficiency as a function of wavelength at different polarizations of the incident light. In the simulations $h = 50$ nm, $w_t = 30$ nm and $w_b = 50$ nm

According to the figure, as the polarization is varied, the peak at about 160 nm remains almost unchanged, indicating the independence on the light's polarization. Interestingly, as φ_p is increased from 0 to 90°, the peak at around 300 nm gradually decreases, while the peak at about 600 nm becomes more pronounced.

To demonstrate the plasmonic modes in more detail, the electric fields with several typical polarizations (i.e., $\varphi_p = 0$, 45, and 90°) were further determined, and the results are summarized in Fig. 7.

a   b   c

Fig. 5. Electric field distribution in the x-y plane with $wb/wt = 2.33$: a – peak A; b – peak B1; c – peak B2

Fig. 7. Electric field distribution in the *x-y* plane with: a and b – $\varphi_p = 0°$; c and d – $\varphi_p = 45°$; e and f – $\varphi_p = 90°$

Note that the wavelengths were 160 and 310 nm for Fig. 7 a and b, respectively; 160 and 360 nm for Fig. 7 c and d, respectively; 160 and 590 nm for Fig. 7 e and f, respectively. By examining Fig. 7 a, c and e, as the polarization angle of the incident light is increased from 0 to 90°, the field of the I-shaped nanostructure is gradually moved from the sides of the post to the surfaces of the bars, corresponding to the rotation of the polarized incident light from the *x*-axis to the *y*-axis. Fig. 7 b, d, and f show that with varying the polarization from 0 to 90°, the field surrounding the surface of the bottom bar is substantially enhanced, which is responsible for the increase of the resonance peak occurring at the longer wavelength (e.g., 590 nm when $\varphi_p = 90°$).

4. CONCLUSIONS

In this paper, an I-shaped rhodium nanomaterial has been investigated in the UV-visible spectrum via the FDTD method. By respectively varying the height of the post, the width ratio of the bottom bar to top bar, as well as the light's polarization, the scattering efficiency and the corresponding electric field of the rhodium nanostructure have been simulated. It has been found that multiple plasmonic resonances can be excited in different wavelength regions, especially in the UV band. In addition, the electromagnetic modes are also revealed, correlating to different resonance peaks. Based on the quantitative analysis of the peak intensity values, it has been shown that the intensities of certain peaks can be systematically adjusted. The peak

intensity of peak B can be enhanced by shortening the height of the post, while increasing the length ratio of the bottom bar to the top bar in the I-shaped structure can effectively increase the peak intensity of peak B_2. This I-shaped structure may be implemented in nanoantenna and metal-enhanced fluorescence. The generation of high-intensity electric fields between nanorods provides a potential platform for the applications of the above fields. This work provides us with a theoretical basis for the design of rhodium-based optical nanomaterials in the UV-visible spectrum.

REFERENCES

1. **Ozbay, E.** Plasmonics: Merging Photonics and Electronics at Nanoscale Dimensions *Science* 311 2006: pp. 189–193.
https://doi.org/10.1126/science.1114849

2. **Fort, E., Gresillon, S.** Surface Enhanced Fluorescence *Journal of Physics D: Applied Physics* 41 (1) 2008: pp. 013001.
https://doi.org/10.1088/0022-3727/41/1/013001

3. **Ebrahimi, S.** Highly Q-factor Elliptical Absorber with Cross Slot as Refractive Index Sensor in Optical Spectrum *Journal of Applied Physics* 53 (7) 2021: pp. 366.
https://doi.org/10.1007/s11082-021-03023-6

4. **Qu, B., Wang, X.G., Li, B., Chen, P.Q., Nie, Q.Y.** Surface Plasmon Resonance Intensification by Cavity-Ring Plasma Structure in the Giga-Hertz Regime *Plasmonics* 15 (6) 2020: pp. 1591–1597.
https://doi.org/10.1007/s11468-020-01180-0

5. **Barnes, W.L., Dereux, A., Ebbesen, T.W.** Surface Plasmon Subwavelength Optics *Nature* 424 2003: pp. 824–830.
https://doi.org/ 10.1038/nature01937

6. **Kauranen, M., Zayats, A.V.** Nonlinear Plasmonics *Nature Photonics* 6 2012: pp. 737–748.
https://doi.org/10.1038/nphoton.2012.244

7. **Gao, Y.H., Wang, J., Wang, W.N., Zhao, T.T., Cui, Y.Y., Liu, P.P., Xu, S.H., Luo, X.L.** More Symmetrical "Hot Spots" Ensure Stronger Plasmon-Enhanced Fluorescence: From Au Nanorods to Nanostars *Analytical Chemistry* 93 (4) 2021: pp. 2480–2489.
https://doi.org/10.1021/acs.analchem.0c04518

8. **Mandal, P.** H-Shape Plasmonic Metasurface as Refractive Index Sensor *Plasmonics* 10 (2) 2015: pp. 439–445.
https://doi.org/10.1007/s11468-014-9825-x

9. **Stokes, N., Cortie, M.B., Davis, T.J., Andrew, M.M.** Plasmon Resonances in V-Shaped Gold Nanostructures *Plasmonics* 7 2012: pp. 235243.
https://doi.org/10.1007/s11468-011-9299-z

10. **Sun, B., Zhao, L.X., Wang, C., Yi, X.Y., Liu, Z.Q., Wang, G.H., Li, J.M.** Tunable Fano Resonance in E-Shape Plasmonic Nanocavities *Journal of Physical Chemistry C* 118 (43) 2014: pp. 25124–25131.
https://doi.org/10.1021/jp4105882

11. **Kim, J.W., Yoo, S.J., Kim, J.M., Choi, S.W., Kim, J.R., Park, S.J., Park, D.J., Nam, J.M., Park, S.H.** Synthesis and Single-Particle Surface-Enhanced Raman Scattering Study of Plasmonic Tripod Nanoframes with Y-Shaped Hot-Zones *Nano Letters* 20 (6) 2020: pp. 4362 – 4369. https://doi.org/10.1021/acs.nanolett.0c01084

12. **Khurana, K., Jaggi, N.** Localized Surface Plasmonic Properties of Au and Ag Nanoparticles for Sensors: A Review *Plasmonics* 16 2021: pp. 981 – 999. https://doi.org/10.1007/s11468-021-01381-1

13. **Zhang, X., Li, P., Barreda, A., Gutierrez, Y., Gonzalez, F., Moreno, F., Everitt, H.O., Liu, J.** Size-tunable Rhodium Nanostructures for Wavelength-Tunable Ultraviolet Plasmonics *Nanoscale Horizons* 1 (1) 2016: pp. 75 – 80. https://doi.org/10.1039/c5nh00062a

14. **Alcaraz, O.R., Sanz, J.M., Barreda, A.I., Saiz, J.M., Gonzalez, F., Everitt, H.O., Moreno, F.** Rhodium Tripod Stars for UV Plasmonics *Journal of Physical Chemistry C* 119 (22) 2015: pp. 12572 – 12580. https://doi.org/10.1021/acs.jpcc.5b00983

15. **Yael, G., Francisco, G., Fernando, M.** The UV Plasmonic Behavior of Rhodium Tetrahedrons-A Numerical Analysis *Applied Sciences* 9 (19) 2019: pp. 3947. https://doi.org/10.3390/app9193947

16. **Watson, A.M., Zhang, X., Alcaraz, O.R., Marcos, S.J., Gonzalez, F., Moreno, F., Finkelstein, G., Liu, J., Everitt, H.O.** Rhodium Nanoparticles for Ultraviolet Plasmonics *Nano Letters* 15 (2) 2015: pp. 1095 – 1100. https://doi.org/10.1021/nl5040623

17. **Gutierrez, Y., Ortiz, D., Saiz, J.M., Gonzalez, F., Everitt, H.O., Moreno, F.** The UV Plasmonic Behavior of Distorted Rhodium Nanocubes *Nanomaterials* 7 (12) 2017: pp. 425. https://doi.org/10.3390/nano7120425

18. **Ahmadivand, A., Sinha, R., Kaya, S., Nezih, P.** Rhodium Plasmonics for Deep-Ultraviolet Bio-Chemical Sensing *Plasmonics* 11 (3) 2016: pp. 839 – 849. https://doi.org/10.1007/s11468-015-0117-x

19. **Zettsu, N., McLellan, J.M., Wiley, B., Yin, Y.D., Li, Z.Y., Xia, Y.N.** Synthesis, Stability, and Surface Plasmonic Properties of Rhodium Multipods, and Their Use as Substrates for Surface-Enhanced Raman Scattering *Angewandte Chemie International Edition* 45 (8) 2006: pp. 1288 – 1292. https://doi.org/10.1002/anie.200503174

20. **Nooshnab, V., Golmohammadi, S.** Conductive Substrate-Mediated Fano Resonances in Aluminum Truncated Hollow Bowtie Nanoantenna Across the Ultraviolet *Optical and Quantum Electronics* 48 (3) 2016: pp. 192. https://doi.org/10.1007/s11082-016-0474-5

21. FDTD Solutions, www.lumerical.com.

22. **Palik, E.D.** Handbook of optical constants of solids. Academic press, 1998: Vol. 3.

23. **Cui, Y., Zhou, J., Tamma, V.A., Park, W.** Dynamic Tuning and Symmetry Lowering of Fano Resonance in Plasmonic Nanostructure *ACS Nano* 6 (3) 2012: pp. 2385 – 2393. https://doi.org/10.1021/nn204647b

24. **Jin, L., Chen, Q., Song, S.C.** Plasmonic Waveguides with Low Polarization Dependence *Optics Letters* 38 (16) 2013: pp. 3078 – 3081. https://doi.org/10.1364/OL.38.003078